Regular Article

ANALYTICAL
AND BIOANALYTICAL
CHEMISTRY
RESEARCH

Published by the
Iranian Chemical Society

***Anal. Bioanal. Chem. Res.**, Vol. 10, No. 3, 269-278, July 2023.*

Electrochemical Sensor Based on Molecularly Imprinted Copolymer for Selective and Simultaneous Determination of Ascorbic Acid and Tyrosine

Zahra Mirzaei Karazan and Mahmoud Roushani*

Department of Chemistry, Ilam University, P. O. Box: 69315-516, Ilam, Iran

(Received 16 December 2022, Accepted 30 January 2023)

This study reported an electrochemical sensor based on molecularly imprinted polymer (MIP) for simultaneous and selective detection of ascorbic acid (AA) and tyrosine (Tyr). The MIP film was electropolymerized on the glassy carbon electrode (GCE) using o-aminophenol (o-AP) and m-dihydroxy benzene (m-DB) as monomers and the dual analyte of AA and Tyr, and its electrochemical performance was evaluated. Influencing parameters such as the pH value, electropolymerization cycle numbers, and template/monomer ratio were optimized. The differential pulse voltammetry (DPV) technique was used for the simultaneous and individual determination of AA and Tyr in their binary mixture. The introduced sensor showed the linear concentration ranges of 0.1-300 μM for AA and 0.01-180 μM for Tyr and good limits of detection were 0.03 μM and 0.003 μM, respectively. The proposed sensor was successfully employed to detect AA and Tyr in real sample. The recoveries were from 98.6 to 102.4% and the RSD was less than 3.5% which exhibited the usability of this sensor in the real sample.

Keywords: Ascorbic acid, Tyrosine, Molecularly imprinted polymer, Electrochemical sensor, Electropolymerization

INTRODUCTION

Tyrosine (Tyr) is a significant and nonessential amino acid with crucial significance to the human body that is produced from phenylalanine in the body [1,2]. Its presence is very essential as responsible for regulating protein synthesis and functions as a precursor for the neurotransmitters containing epinephrine, norepinephrine, and dopamine [3]. An abnormality in the level of Tyr leads to depression and various diseases including albinism, alkaptonuria, Parkinson's, liver disease, tyrosinemia, mental illness, and lung disease [4-6]. Ascorbic acid (AA) or ascorbate, also called vitamin C, is a significant water-soluble vitamin essential in human nutrition derived from fruits and green vegetables [7,8]. It plays an important role in the defense of the immune generally [9]. AA helps the establishment of collagen in teeth, bones, tissues, blood vessels, cartilages, and skin plays a role in detoxifying the body from toxic metals, healing wounds, decreasing histamine levels, necrosis, and facilitating apoptosis, increasing antibody levels, and acts as an antioxidant [10, 11]. Cardiovascular diseases, Alzheimer's and Parkinson's diseases, scurvy, and cancer are caused by abnormal levels of ascorbic acid [12,13]. In recent years, various electrochemical methods with chemically modified electrodes for an individual determination of AA and Tyr have been reported [14-19]. The dual analyte of AA and Tyr are coexisting in biological fluids including serum. Monitoring the concentration of AA and Tyr in body fluids is essential to diagnose diseases. Therefore, a selective, fast, and low-cost technique for the simultaneous determination of these templates is a necessary step.

In recent years, molecularly imprinted polymer (MIP) technique-based electrochemical sensor has attracted excessive attention as a particular recognition tool according to the binding of paired cavities in shape and size to the analytes for improving the selectivity of sensors [20 -22]. Several polymerization techniques such as sol-gel,

*Corresponding author. E-mail: m.roushani@ilam.ac.ir

electropolymerization, layer-by-layer deposition, and bulk polymerization have been used in preparing MIP sensors [23]. An electropolymerization method, in comparison to other techniques, is an effective tool for decorating the MIP film on the electrode surface. It has good properties, including rapid and easy preparation, inexpensive, desirable sensitivity, selectivity detection, *etc*. [24].

In this research, a new electrochemical sensor was designed based on the MIP sensor through an easy electropolymerization technique. The dual analyte of AA and Tyr in conjugation with o-aminophenol (o-AP) and m-dihydroxy benzene (m-DB) as monomers was used in the polymerization solution preparation stage. The introduced MIP sensor showed excellent sensitivity and selectivity in the simultaneous detection of analytes. Furthermore, a prepared MIP sensor was employed in the serum sample with admissible results. According to our knowledge, research on selective, sensitive, and simultaneous determination based on the dual-MIP sensor toward AA and Tyr is yet relatively rare.

EXPERIMENTAL

Materials and Apparatus

KCl, $[Fe(CN)_6]^{3-/4-}$, m-DB, o-AP, AA (99%), and Tyr (99%) were purchased from Sigma-Aldrich. Electrochemical experiments were performed in a phosphate buffer solution (PBS, 0.1 M, pH = 7.4), which was prepared using NaH_2PO_4 and Na_2HPO_4.

A Voltalab EIS/potentiostat/galvanostat electrochemical analyzer (ZIVE Lab sp1, Korea) equipped with a three-electrode cell was applied for the electrochemical data such as differential pulse voltammetry (DPV), electrochemical impedance spectroscopy (EIS), and cyclic voltammetry (CV). Platinum electrode, Ag/AgCl electrode, and glassy carbon electrode (GCE) were used as the counter, reference, and working electrodes, respectively. Fourier transform infrared spectroscopy (FTIR) was employed to verify the accuracy of the created sensor. The surface morphology of modified electrodes was performed using a scanning electron microscope (SEM).

Preparation of MIP Film on the Electrode Surface

The MIP synthesis stages was illustrated in Fig. 1. Before electropolymerization, the GCE was polished with alumina slurry. The bare GCE was placed in PBS (pH = 7.4) including the dual analyte (0.05 mM of AA and Tyr) and the monomers (0.5 mM of m-DB and o-AP). The electropolymerization was executed by CV through 10 consecutive cycles at 50 mV s^{-1} in the potential range from -0.1 V to 1 V. The particular binding sites on the MIP film were created after eliminating the analytes via washing with a solution of nitric acid-doubly distilled water (1:1) for 2 min. The non-imprinted polymer (NIP) was obtained using the same experimental conditions without the addition of analytes.

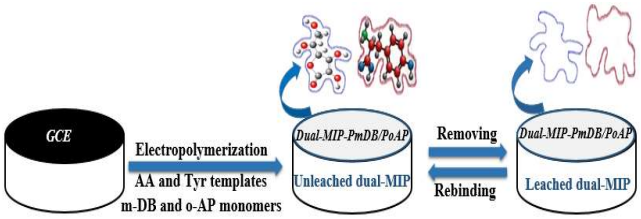

Fig. 1. Schematic from the preparation process of the dual-MIP sensor.

Fabrication of Real Sample

The human serum sample was taken from the clinical laboratory. Initially, methanol (2 ml) was added to the serum sample (1.5 ml) to extract the interfering proteins. After vortexing the serum (2 min), the precipitated proteins were separated by centrifugation at 4000 rpm. The supernatant was filtered and diluted with PBS (0.1 M, pH = 7.4) [25,26].

RESULTS AND DISCUSSION

Characterization of Dual-MIP-PmDB/PoAP-GCE

The affirmation of the configuration of the dual-MIP film on GCE was investigated through the SEM technique (Fig. 2). The dual-MIP-PmDB/PoAP-GCE presented a rough surface and was covered via many slices (Fig. 2A), illustrating the successful modification of MIP film. The rough surface provided a wide particular surface area for the detection and recognition of AA and Tyr. As exhibited in Fig. 2B, after eluting the dual template, the MIP surface is rough and full of many cavities, but the slices disappeared, indicating that the templates were extracted from the polymer layer. A comparison of the dual-MIP film morphology before

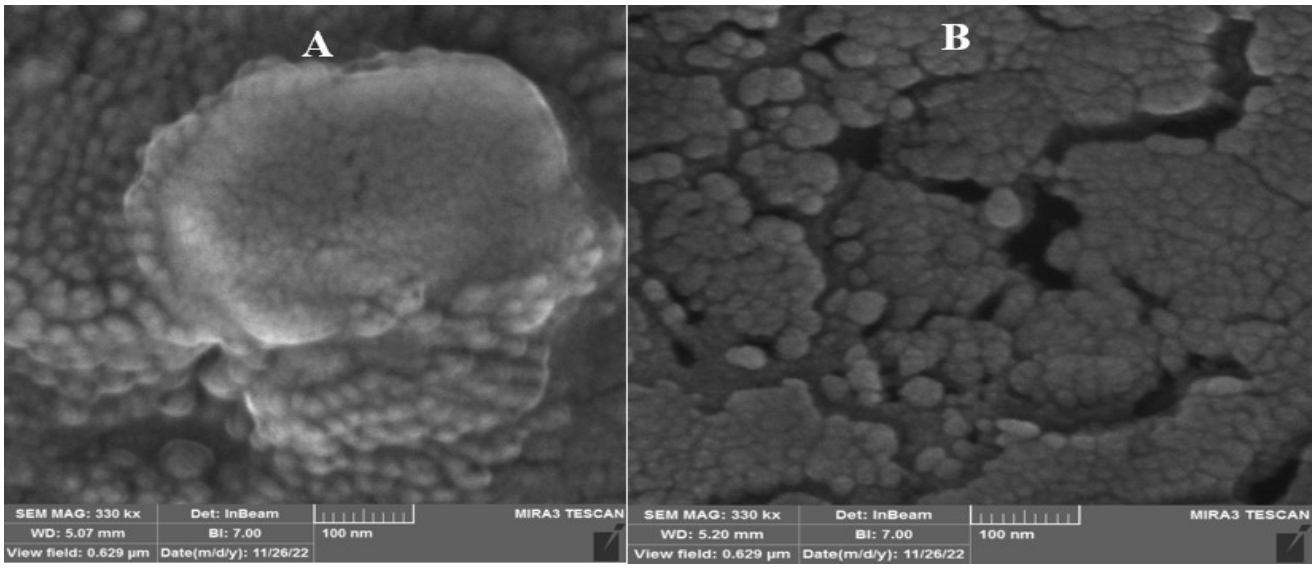

Fig. 2. SEM images of (A) un-leached dual-MIP and (B) leached dual-MIP.

and after the elimination of the dual analyte highlights the architecture of copious imprinted sites following the elimination step.

Additionally, before and after extracting the dual template, FTIR spectroscopy was performed to further evaluate the accuracy of the sensor (Fig. 3). As anticipated, the characteristic bonds of the dual-MIP layer were declared in all substances. The bond remarked at 3446 cm^{-1} related to the OH, its intensity decreased after dual analyte elimination, providing the interaction of monomers and analytes. The bond shown at 2458 cm^{-1} is proportion to the carbonyl region, which its intensity was decreased after the removal of analytes compared to before. The peak at 1735 cm^{-1} is related to the Ester group. It decreased after the washing step. The bond that appears at 1483 cm^{-1} for C=C belongs to the aromatic ring bending vibrations, decreasing peaks intensity in leached polymer severely that proved dual template elimination. The achieved results of the FTIR analysis assured that there were not both AA and Tyr in the leached dual-MIP film.

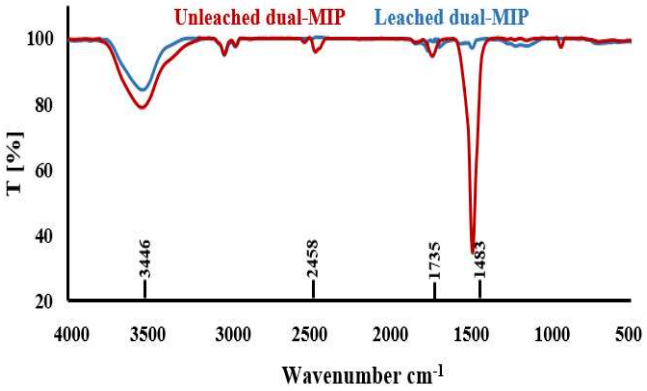

Fig. 3. The FTIR spectra of un-leached and leached dual-MIP film.

Electrochemical Characterization of the Modified Electrodes

The CV behavior of the various modified electrodes was recorded in a 5 mM $[Fe(CN)_6]^{3-/4-}$ probe (Fig. 4A). After the electropolymerization stage, the peak current of dual-MIP has greatly reduced as compared to the bare GCE (curve a), illustrating that the electropolymerization has been favorably coated on the electrode (curve b) and this has caused the blocking of the electron transfer from the solution. After eliminating the dual template via the eluting solution, because sites were created on the MIP layer to transfer the electrons, the current response reappeared (curve c) as compared to curve b. Subsequently, the NIP-PmDB/PoAP-GCE was evaluated (curve d), indicating the insulating characterization of the NIP layer and an extreme reduction in the current response.

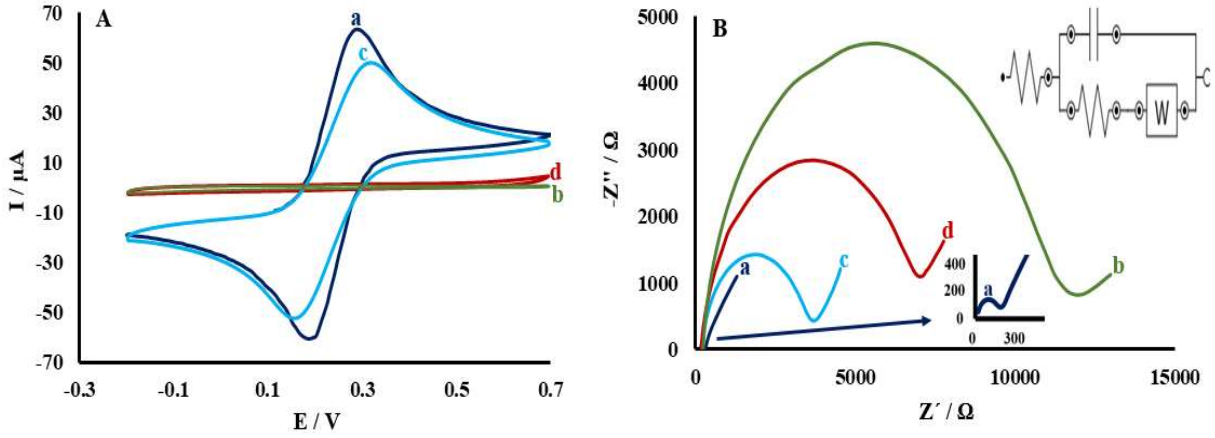

Fig. 4. (A) CV and (B) EIS results of bare GCE (a), dual-MIP-PmDB/PoAP-GCE before (b) and after (c) removing the dual template, and NIP-PmDB/PoAP-GCE (d) in 0.1 M KCl, 5 mM of $[Fe(CN)_6]^{3-/4-}$ solutions. The Platinum electrode, Ag/AgCl (saturated KCl) electrode, and GCE were used as the counter, reference, and working electrodes, respectively.

EIS method was applied to characterize the modified electrodes using the probe of 5 mM $[Fe(CN)_6]^{3-/4-}$ (Fig. 4B). The charge transfer resistance (Rct) values severely incremented from 305.2 Ω (curve a) to 13164.7 Ω (curve b) when the dual-MIP film was deposited on GCE because the dual-MIP layer led to the lower transfer of the electron. The Rct was reduced to 3823.5 Ω after template extraction (curve c) due to the making of particular recognition cavities that decreased the resistance to the transfer of electrons. Lastly, the resistance incremented (Rct = 7385.4 Ω) for NIP-PoAP/PmDB-GCE (curve d) because the polymeric matrix conductivity was reduced. The obtained results of EIS were in accordance with CV measurements.

Optimization of the Factors for MIP Sensor Preparation

To obtain an incomparable output of the designed dual-MIP sensor; a series of factors, including cycle numbers, template/monomer ratio, and pH value of PBS were evaluated.

The scanning cycles, an important parameter, can sorely affect the thickness of the dual-MIP film. Figure 5A illustrates the DPV current responses of 10 µM AA and 1 µM Tyr (curve a and curve b) that were achieved from a dual-MIP sensor in various electropolymerization scanning cycles. It is exhibited when the cycle number was 10, and the maximum current responses of analytes were obtained. Besides, the peak currents of the dual template on the MIP layer first increased and then decreased, when the cycle number was over 10 the thicker MIP layer was achieved, and when it was less than 10, the thinner MIP film resulted. As the result, 10 cycles was selected as the optimal number of cycles.

To optimize the mole ratio of dual template to monomers, because it has a significant role in the MIP structure and the rebinding affinity, various template/monomer ratios including 1:10, 1:15, 1:20, 1:25, and 1:30 were appraised while the concentration of the analytes was kept at 0.05 mM, and the DPV current responses of the dual-MIP-PmDB/PoAP-GCE after every electropolymerization was taken. According to Fig. 5B, the current response increased with the template/monomer ratio, until it remained constant at a 1:20 ratio. Thus, the template/monomer ratio was chosen as 1:20 for dual-MIP synthesis.

The pH as another effective parameter was investigated since its value affects the detection ability, the interaction between the monomers and dual template, and the peak current response. Figure 5C affirmed the DPV current responses of 10 µM AA and 1 µM Tyr (curve a and curve b) achieved at various pH values from PBS. Here, as the pH incremented to 6-7.4, the peak current of templates on the dual-MIP layer increased, and, then, decreased with an extra increasing the pH value. Tyr includes several functional groups which ionize at various pH values. Distinct tyrosine forms are possible such as $R^{-\,-}$, R^{-}, R, and R^{+} [27,28]. At pH = 7.4, the carboxyl group in Tyr exists as an anion form,

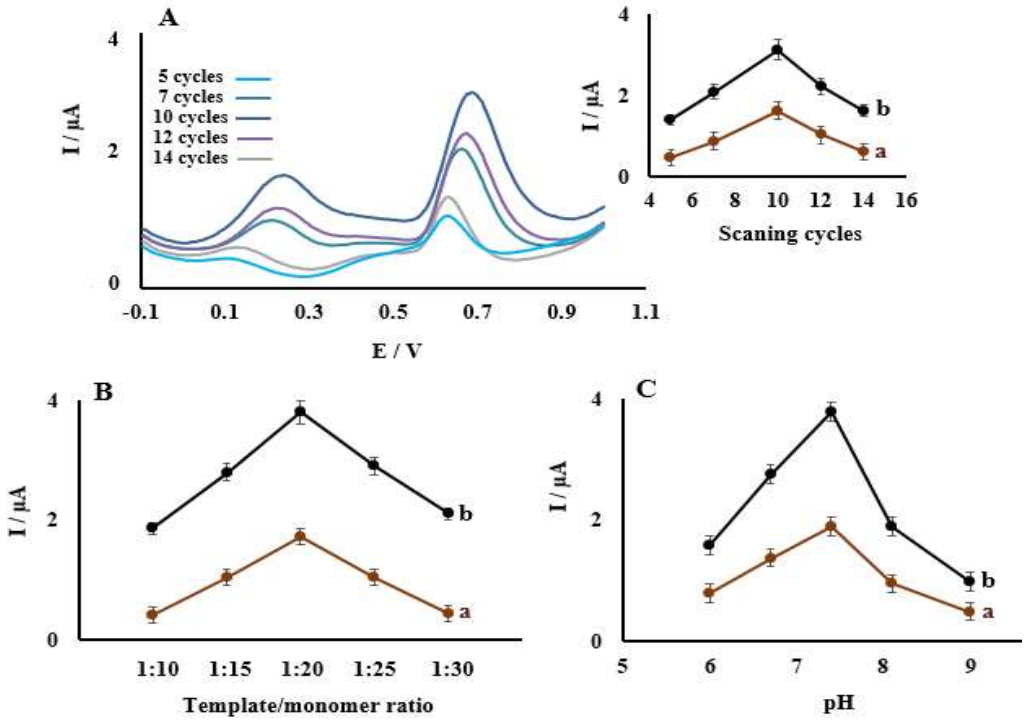

Fig. 5. Effects of (A) electropolymerization scanning cycles, (B) template/monomer ratio, and (C) pH value on the peak currents of 10 µM AA (a) and 1 µM Tyr (b) (n = 4).

so Tyr appears in a form with a negative charge. The electrostatic attraction between the polymer film and the carboxyl group of Tyr can result in a high DPV current at pH = 7.4. Nevertheless, as the values of the pH increased to the basic region, the polymer film became negatively charged [5,18]. The electrostatic repulsion played a leading role between Tyr and the polymer film, which led to a gradual reduction in the DPV response of the Tyr. In addition, the oxidation of AA at pH < 8 possesses two consecutive one-electron oxidation stages, illustrating the bioelectronic process in which two protons interchange at pH 2-4.5, one proton at pH 4.5-8, and two protons at pH > 8 [29-31]. At pH values of 4.5-8, one proton interchange, with ascorbate anion as electroactive species. It was found that the intermediate, ascorbate anion is electrochemically oxidized to a diketolactone, consequently dehydrated to dehydroascorbic acid that rearranges to another ene-diol further oxidized at higher potentials [29,32]. Therefore, at pH = 7.4, AA appears in an anion form that is easily oxidized and increased the current response. Then, pH = 7.4 of PBS was used for the electrochemical measurements.

Electrochemical Properties of AA and Tyr on the Modified Electrodes

The CV curves of AA and Tyr on the modified electrodes in PBS (pH = 7.4) shows in Fig. 6. At the bare electrode, petty oxidation peaks were illustrated for AA and Tyr due to the slow rate of electron transfer (curve a). After electropolymerization, at dual-MIP-PmDB/PoAP modified electrode (curve b), the current responses of analytes increased severely which can be attributed to the synergistic electrocatalytic issue on the dual-MIP film. The dual-MIP layer provided the particular binding holes that improve the absorption efficiency of analytes on GCE. In other words, the dual template can be easily absorbed in the proper cavities in the MIP film, the electron transfer between the dual target and electrode was also accelerated and resulted in the enlarged current responses. A comparison of the NIP electrode was also assayed (curve c). After modification with NIP, weak oxidation peaks resulted due to the lack of particular binding holes for the analytes.

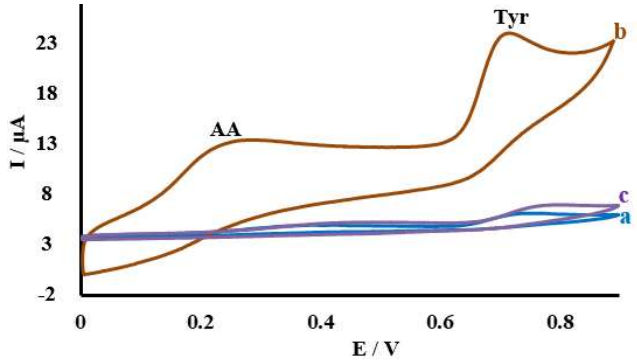

Fig. 6. CV curves of 200 µM AA and 100 µM Tyr at bare GCE (a), MIP modified electrode (b), and NIP modified electrode (c) in PBS (pH = 7.4). The potential scan rate is 100 mV s^{-1}.

Selective Detection from AA and Tyr

In order to confirm the feasibility of the simultaneous detection of AA and Tyr through the dual-MIP-PmDB/PoAP-GCE, the DPVs performed in the mixtures when the concentration of one analyte changed and another was held constant. Figure 7A indicates that the peak current for the AA increases linearly with the increment of its concentration, while the peak response for Tyr holds almost unchanged (Tyr: 60 µM). This exhibits that Tyr has no interfering effect on the determination of AA. Similarly, Fig. 7B displays that with the increase in Tyr concentration, the peak responses of Tyr show a linear increase, while the peak responses for AA are nearly constant (AA: 100 µM), which proposes that the presence of AA does not interfere with the response of Tyr. All the results severely signify that AA and Tyr can be individually determined in their mixture using the suggested technique.

Analytical Application

270 analytical application of the dual-MIP sensor was examined via the simultaneous detection of AA and Tyr. Figure 8A shows DPV responses of the dual analyte on the dual-MIP sensor, illustrating that the oxidation current responses of AA and Tyr incremented simultaneously with the enhancing concentrations. As result, the peak currents were proportional to AA and Tyr concentrations in the ranges of 0.1-300 µM and 0.01-180 µM, respectively. The linear regression equations were described as I (µA) = 0.567 (µM) + 5.1989 (R^2 = 0.9989) for AA, and I (µA) = 0.921 (µM) + 9.5072 (R^2 = 0.9992) for Tyr (Fig. 8B and Fig. 8C). In this study, the detection limit (LOD) was obtained based on S/N = 3. The LOD was calculated as 0.03 µM for AA and 0.003 µM for Tyr. Then, the dual-MIP sensor displayed two linear regression equations at different concentration ranges with low LODs. Moreover, Comparative results of the dual-MIP sensor and formerly reported studies are summarized in Table 1. The introduced sensor displayed a wider linear range and lower LODs for the simultaneous determination of AA and Tyr.

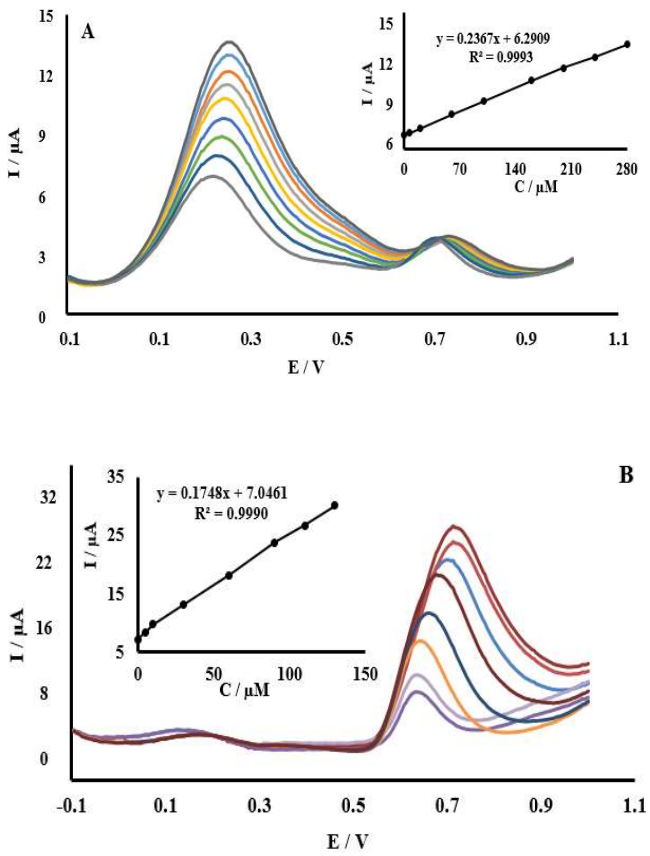

Fig. 7. DPV curves of dual-MIP-PmDB/PoAP-GCE in pH 7.4 of PBS (A) including 60 µM Tyr and various concentrations of AA (0.05, 0.5, 20, 60, 100, 160, 200, 240, and 280 µM). (B) Including 100 µM AA and different concentrations of Tyr (0.01, 2, 10, 30, 60, 90, 110, and 130 µM). Inset: designs of the peak current as a function of AA and Tyr concentrations.

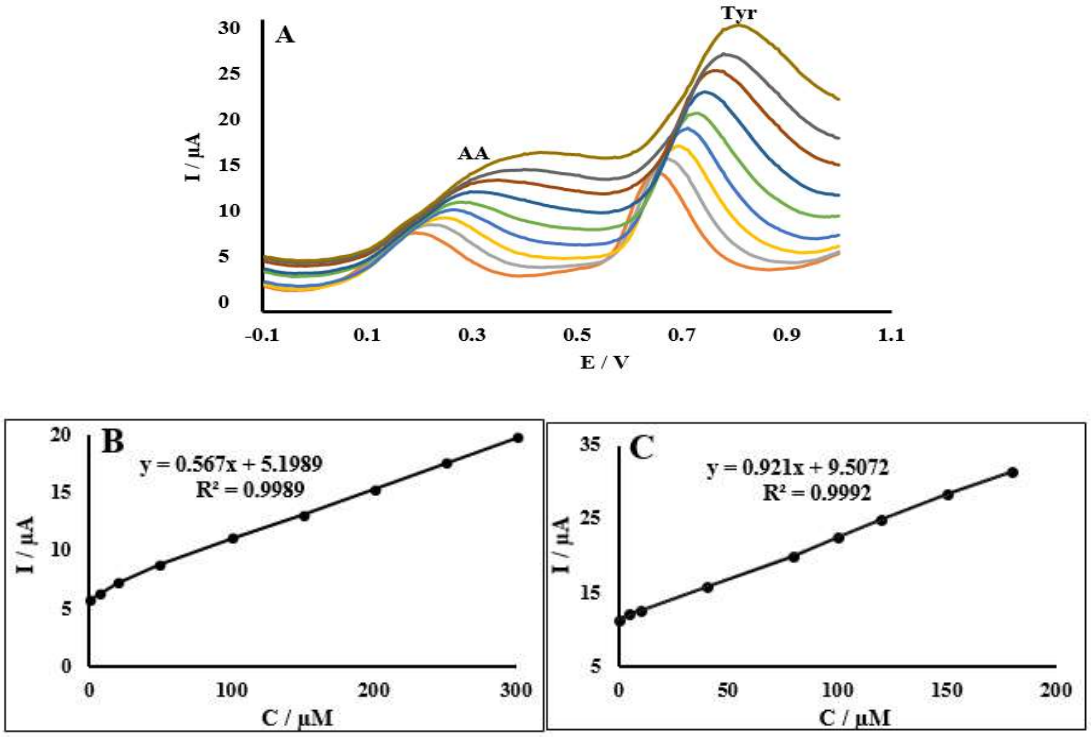

Fig. 8. (A) DPV curve of various concentrations of AA and Tyr at the dual-MIP sensor (n = 4). The calibration curve corresponding to (B) AA in the concentration range including 0.1, 1, 15, 50, 100 150, 200, 250, and 300 µM and (C) Tyr in the concentration range including 0.01, 0.1, 8, 40, 80, 100, 120, 150, and 180 µM.

Table 1. Comparison with Electrochemical Sensors for the Determination of AA and Tyr

Modified electrode	Analyte	Method	Linear range (µM)	LOD (µM)	Ref.
PVP-GR/GCE	AA	LSV	4-1000	0.8	[33]
Fe3O4NPs@SPCE	AA	SWV	10-100	15.7	[34]
ITO-rGO-AuNPs	AA	LSV	20-100	5.63	[35]
GR/Au NPs/GCE	Tyr	LSV	0.1-100	0.047	[36]
Al-CuSe-NPs/SPCE	Tyr	LSV	0.15-10	0.04	[37]
EGr/GC	Tyr	LSV	6-1000	0.81	[38]
Dual-MIP	AA & Tyr	DPV	0.1-300 & 0.01-180	0.03 & 0.003	This work

Selectivity, Repeatability, Reproducibility, and Stability of the Sensor

The selectivity was investigated *via* the DPV technique of 10 µM of AA and Tyr in the presence of 100-fold of various interference compounds with the same properties or structures such as sucrose, glucose, fructose, urea, citric acid, and starch. As exhibited in Fig. 9, the high peak currents to AA and Tyr at dual-MIP-PmDB/PoAP-GCE without

apparent responses to the interfering compounds indicates that the dual template can be recognized in presence of interference substances because the imprinted membranes were the specific detection cavities to the analytes and the other compounds have no effect on the detection of AA and Tyr, indicating that the dual-MIP sensor possesses a good anti-interference characteristic in the determination of AA and Tyr so the admissible selectivity of this sensor was evolved from the MIP film that can be related to the particular binding cavities on it.

Repeatability was measured by detecting 10 µM of AA and Tyr for 10 measurements on the same designed sensor. Gratifying repeatability was achieved with the relative standard deviation (RSD, n = 10) of 3.4% and 2.9% for AA and Tyr, respectively. The reproducibility was obtained by detecting 10 µM of AA and Tyr using 5 various MIP sensors prepared under the same experimental conditions. The RSD was calculated to be 2.6% and 3.5% for AA and Tyr, respectively, showing good reproducibility of the sensor. In addition, more than 90% of the initial sensor response was retained after placing for 21 days at 5 °C, indicating the suitable stability of the sensor.

Sample Analysis

The dual-MIP-PmDB/PoAP sensor was applied in the recognition of AA and Tyr in a serum sample by the DPV technique and standard addition method to illustrate the applicability of the present technique. The sample was treated as described in the section on the fabrication of real sample and any case undergoes three measurements. The results were briefed in Table 2. The recoveries were from 98.6 to 102.4% and the RSD was less than 3.5% which exhibited the usability of this sensor in the actual sample.

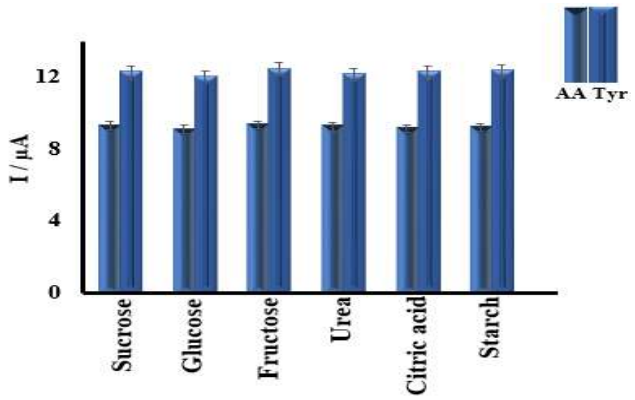

Fig. 9. The selectivity of the dual-MIP sensor in detecting AA and Tyr in the presence of interference substances.

CONCLUSIONS

In the present research, a selective and simultaneous determination of AA and Tyr using dual-MIP-PmDB/PoAP-GCE film through the electropolymerization method was accomplished for the first time. Herein, we reported the application of a novel, rapid, simple, and selective electrochemical sensor based on AA and Tyr molecularly imprinted membrane on GCE. The electrochemical performance of the sensor can be adjusted via optimization of the parameters in the MIP synthesis process. Peak separation of AA and Tyr could be achieved using DPV, demonstrating that the dual-MIP-PmDB/PoAP-GCE facilitated their individual and simultaneous detection. According to the results, the introduced sensor exhibited the linear concentration ranges of 0.1-300 µM for AA with LOD 0.03 µM and 0.01-180 µM for Tyr with LOD 0.003 µM. The total assay time of the developed sensor was less than 10 min. Under the optimal condition, the designed sensor

Table 2. Determination of AA and Tyr in the Real Sample (n =3)

Sample	Templates	Added (µM)	Found (µM)	Recovery (%)	RSD (%)
	AA	-	25.0	-	2.8
	AA	10	34.5	98.6	3.5
Serum	AA	100	128.0	102.4	1.9
	Tyr	-	12.5	-	3.3
	Tyr	10	21.7	96.5	3.4
	Tyr	100	113.0	100.5	2.6

demonstrates high selectivity, desirable repeatability and reproducibility, good stability, and usability in the real sample with acceptable recoveries ranging from 98.6 to 102.4% and the RSD being less than 3.5%. As result, the present sensor can be simply employed and extended as a rapid and selective diagnostic technique to detect a range of substances in the healthcare area at quality control laboratories in the future.

Supplementary Information

A brief description of any additional material omitted from the main body in the interest of presenting a clearer and more readable manuscript.

REFERENCES

[1] M.S. Attia, A.A. Yakout, RSC Adv. 6 (2016) 20467.

[2] C.C. Negut, C. Stefanov, J. Frederick van Staden, Electroanalysis 32 (2020) 1488.

[3] Z. Galla, C. Rajda, G. Racz, N. Grecso, A. Barath, L. Vecsei, C. Bereczki, P. Monostori, J. Chromatogr. A. 1635 (2021) 461775.

[4] C. Mocanu, A. Bocec, R. Gradinaru, D. Anton-Paduraru, Approach 71 (2020) 285.

[5] W. Zheng, M. Zhao, W. Liu, Sh. Yu, L. Niu, G. Li, H. Li, W. Liu, J. Electroanal. Chem. 813 (2018) 75.

[6] O.J. D'Souza, R.J. Mascarenhas, A.K. Satpati, I.N.N. Namboothiri, S. Detriche, Z. Mekhalif, J. Delhalle, RSC Advances 5 (2015) 91472.

[7] G. Uwaya, O. Fayemi, J. Clust. Sci. 33 (2022) 1.

[8] S. Skrovankova, J. Mlcek, J. Sochor, M. Baron, J. Kynicky, T. Jurikova, Int. J. Electrochem. Sci. 10 (2015) 2421.

[9] Ph. Motsaathebe, O. Ester Fayemi, Nanomaterials 12 (2022) 64.

[10] N. Chauhan, S. Soni, P. Agrawal, Y.P.S. Balhara, U. Jain, Process Biochem. 91 (2020) 241.

[11] P. Gupta, S. Tiwari, J. Haria, Int. J. Sci. Study 1 (2014) 37.

[12] J.G. Manjunatha, B.K. Swamy, M. Deraman, G.P. Mamatha, Int. J. Pharm. Pharm. Sci. 5 (2013) 355.

[13] A.M. Pisoschi, A. Pop, A.I. Serban, C. Fafaneata, Electrochim. Acta 121 (2014) 443.

[14] Sh. Liu, X. Jiang, M. Yang, Microchim. Acta 186 (2019) 1.

[15] K. Dhara, R.M. Debiprosad, Anal. Biochem. 586 (2019) 113415.

[16] Y. Zhang, P. Liu, S. Xie, M. Chen, M. Zhang, Z. Cai, R. Liang, Y. Zhang, F. Cheng, J. Electroanal. Chem. 818 (2018) 250.

[17] P. Deng, J. Xiao, J. Feng, Y. Tian, Y. Wu, J. Li, Q. He, Microchem. J. 170 (2021) 106645.

[18] C. Varodi, F. Pogacean, M. Coros, A. Ciorita, S. Pruneanu, Sens. 22 (2022) 3606.

[19] B. Xiaopeng, W. Ying, D. Lili, G. Li, X. Tianchi, S. Wenbo, F. Xun, Curr. Anal. Chem. 18 (2022) 495.

[20] L. Zhu, Y. Cao, G. Cao, Biosens Bioelectron. 54 (2014) 258.

[21] Z. Mirzaei Karazan, M. Roushani, Anal. Methods 13 (2021) 4904.

[22] B. Qader, I. Hussain, M. Baron, R. Jimenez-Perez, J. Gonzalez-Rodriguez, G. Gil-Ramírez, Electroanalysis 33 (2021) 1129.

[23] M. Arvand, M. Zamani, M. Sayyar Ardaki, Sens. Actuators B 243 (2017) 927.

[24] J.L. Silva, E. Buffon, M.A. Beluomini, L.A. Pradela-Filho, D.A.G. Araujo, A. L. Santos, R.M. Takeuchi, N.R. Stradiotto, Anal. Chim. Acta 1143 (2021) 53.

[25] T. Madrakian, E. Haghshenas, A. Afkhami, Sensors and Actuators B 193 (2014) 451.

[26] M. Roushani, Z. Jalilian, Electroanalysis 30 (2018) 2712.

[27] M.S. Attia, A.O. Youssef, A. Essawy, Anal. Methods 4 (2012) 2323.

[28] M.S. Attiaa, A. Yakout, RSC Adv. 6 **(**2016) 20467.

[29] M. Rueda, A. Aldaz, F. Sanchez-Burgos, Electrochim. Acta 23 (1978) 419.

[30] X. Zhang, M. Wang, D. Li, L. Liu, J. Ma, J. Gong, X. Yang, X. Xu, Z. Tong, J. Solid State Electrochem. 17 (2013) 3177.

[31] A.M. Pisoschi, A. Pop, A.I. Serban, C. Fafaneata, Electrochim. Acta 121 (2014) 443.

[32] G. E. Uwaya1, O.E. Fayemi, J. Clust. 33 (2022) 1035.

[33] Y. Wu, P. Deng, Y. Tian, J. Feng, J. Xiao, J. Li, J. Liu, G. Li, Q. He, J. Nanobiotechnol. 18 (2020) 1.

[34] G.E. Uwaya, O.E. Fayemi, J. Clust. Sci. 32 (2021) 1.

[35] F. Mazzara, B. Patella, G. Aiello, A. O'Riordan, C. Torino, A. Vilasi, R. Inguanta, Electrochim. Acta 388

(2021) 138652.
[36] M. Liu, J. Lao, H. Wang, Z. Xu, J. Li, L. Wen, Z. Yin, C. Luo, H. Peng, Russ. J. Electrochem. 57 (2021) 41.
[37] K. Murtada, R. Salghi, A. Ríos, M. Zougagh, J. Electroanal. Chem. 874 (2020) 114466.
[38] C. Varodi, F. Pogacean, M. Coros, A. Ciorita, S. Pruneanu, Sensors 22 (2022) 3606.